Regression based battery state of health estimation for multiple electric vehicle fast charging protocols

Journal of Power Sources 624 (2024) 235601

Contents lists available at ScienceDirect

Journal of Power Sources

journal homepage: www.elsevier.com/locate/jpowsour

Regression based battery state of health estimation for multiple electric vehicle fast charging protocols

Matteo Acquarone [a,b], Federico Miretti [a,*], Tiziano Alberto Giuliacci [a], Josimar Duque [c], Daniela Anna Misul [a], Phillip Kollmeyer [c]

[a] Energy Department, Politecnico di Torino, Torino, 10138, Italy
[b] Center for Automotive Research and Sustainable Mobility (CARS@PoliTo), Politecnico di Torino, Torino, 10141, Italy
[c] McMaster Automotive Resource Center (MARC), McMaster University, Hamilton, 94305, ON, Canada

HIGHLIGHTS

- Data-Driven SOH Estimation exploiting charging events.
- Robust across different fast charging protocols.
- Robust with respect to SOC estimation errors.
- Validation on extended dataset.
- Low-computational-effort suitable for online BMS.

ARTICLE INFO

Keywords:
SoH
BMS
Fast charging
Data driven

ABSTRACT

In this work, a data-driven estimation method is developed to estimate the battery state of health (SOH), exploiting SOH features that can be obtained during fast-charging events. A newly expanded experimental dataset with six cells, cycled 1200 to 1800 times until 70% SOH is reached, is used and made available. Our investigation focuses on the variability that can be encountered in charging events due to different charging protocols (particularly for fast charging) and partial charging events. In particular, we investigated nine different SOH features, introducing novel formulations to increase their flexibility with respect to different charging events. Then, we assessed the practical implementability of these features and employed correlation and feature importance analyses to identify the most effective. Finally, we developed a linear regression model for SOH estimation using the selected features as inputs. The model shows an RMS prediction error as low as 1.09% over the battery lifetime and a maximum error no greater than 3.5% until SOH falls below 80%, corresponding to the end-of-life for automotive applications. The estimator is also shown to be robust against significant errors of the state of charge (SOC) input value (as high as 5%), ensuring it will perform well even when SOC is not accurately known.

1. Introduction

One of the most prominent technological challenges to the deployment of electric vehicles is the performance of battery packs, which degrades over time. This results in a noticeable reduction in range and energy efficiency as the vehicle age increases. Since limited battery longevity and range have long been understood to be among the most crucial factors impacting customer acceptance of electric vehicles (EV) [1,2], upcoming regulations are expected to set new requirements on battery durability, such as the recently agreed upon limits as part of the Euro 7 package in the European Union [3].

As a result, the issue of battery aging is a cause of great concern and is being addressed by many researchers in the industry and academia. State of health (SOH) estimation algorithms attempt to quantify the battery degradation, typically in terms of capacity fading [4]. These algorithms are developed as part of the battery management system (BMS) both in vehicular and stationary applications for safety and diagnostic purposes, informing the user or operator when the battery degradation has reached a level that would hamper its application, and, therefore, a battery replacement is needed. Furthermore, accurate knowledge of the SOH enables the deployment of smart control

* Corresponding author.
E-mail address: federico.miretti@polito.it (F. Miretti).

https://doi.org/10.1016/j.jpowsour.2024.235601
Received 18 July 2024; Received in revised form 1 October 2024; Accepted 8 October 2024
Available online 14 October 2024

strategies that maximize lifetime. Indeed, it is possible to develop health-conscious battery management systems which adopt control strategies that prolong battery life, e.g., optimizing its thermal management [5,6], charging events [7] and cell balancing [8]. Similarly, health-conscious energy management strategies have been developed for fuel-cell electric vehicles [9] and for hybrid-electric vehicles [10–13], both of which require a battery as a key component.

Existing SOH estimation algorithms broadly fall into two different categories: model-based and data-driven. Model-based approaches typically use Kalman filters [14] or other types of observers [15], combining available measurements (such as the terminal voltage) with a state dynamics model, which is typically based on electrochemical models, e.g., Doyle-Fuller-Newman models and Single Particle Models, or equivalent circuit models (ECM). These approaches offer the highest interpretability since they directly model the physical behavior of battery cells. Data-driven approaches on the other hand do not rely on any physical model and rather attempt to directly link available measurements to the SOH, using statistical methods or machine learning [16]; therefore, they require an experimental dataset [17], which should be large enough to train the data-driven model. One of the main disadvantages of the data-driven models is that they tend to perform poorly when used in operating conditions that vary significantly from those covered in the training dataset. To address this weakness, it is important to both carefully design the experimental campaign to generate a wide training dataset and to ensure that the model is tested over conditions similar to training, leading to reliable estimation. Finally, hybrid methods that combine model-based with data-driven approaches have been developed to retain their benefits and mitigate their weaknesses.

As mentioned above, data-driven methods are most reliable if trained and used with a repeatable duty cycle. This explains why significant attention has been devoted to the charging phase of electric vehicles rather than the actual driving. If a full charging sequence is considered, the current and voltage profiles are typically very effective features of the state of health [18]. Unfortunately, a full charging phase is rarely performed in real operation, whereas partial charging events are frequent. Therefore, data-driven approaches based on charging sequences require the definition of informative features that can be evaluated from partial charging profiles [19].

Another work [20] proposes an SOH estimation approach considering the CC phase of a typical CC–CV charging event. Unlike other techniques, the constant current charging stage is divided into short segments. Then, a single health indicator, corresponding to the charging capacity plus a correction term for the initial charging voltage, is extracted within each short segment. Finally, a kernel ridge regression-based estimator is used. Other approaches rely on the incremental capacity [21] took a different approach: the incremental capacity curves were obtained from the CC phase of a CC–CV charging event, and a portion of the IC curve which is expected to contain a peak is discretized to generate features for an LSTM (Long short-term memory network), a type of recurrent neural network.

Unfortunately, all these works only consider one charging protocol (CC–CV charging) and were only tested with low C-rates. Also, these methods can only be used if the CC charging phase is present and sufficiently long. Finally, none of these works attempt to compare different kinds of health indicators, which is one of the contributions of our work.

In real-life operation, the characteristics of different charging protocols must be taken into account for a SOH estimation algorithm. Since fast-charging procedures are based on the use of high C-rate currents, the charging voltage profiles are quite different from the ones obtained at lower currents. As previously mentioned, most of the published works, such as those mentioned earlier, are designed for the low C-rate constant current–constant voltage (CC–CV) charging strategy; therefore, they have limited applications for electric vehicles. In contrast, fewer works address the complicated problem of SOH estimation for fast-charging applications. Even these, however, fail to account for the high variability in charging protocols, which hinders their application in real-world scenarios where the electric vehicle can be charged using different fast-charging protocols.

The high variability of charging protocols is particularly present in fast-charging applications. Indeed, since higher C-rates lead to a faster aging process, different fast-charging protocols have been proposed in the literature attempting to speed up the overall charging rate while inhibiting the lithium deposition, which is understood to be the primary cause of aging in charging operations [22]. Examples of non-standard fast-charging protocols are the multi-stage charging currents (MSCC) protocols [23] and pulse charging (PC) profiles, which alternate charging currents to discharging [24] or rest [25] pulses.

Therefore, it is important to develop robust features and algorithms that can be applied to any charging profile for real-world SOH estimation. However, most of the works tackle the SOH estimation problem during fast-charging by assessing the estimation model capability over a single fast-charging protocol. The authors of [26] use a long short-term memory neural network that takes as input the current, voltage, and temperature signals to estimate SOH with the data collected during the battery charging process. The model is trained and tested using only measurements from the constant current charging phase.

Some works [27,28] attempt to formulate more general SOH features that can be computed for an MSCC fast-charging protocol featuring the same phases but with different durations and current levels for each constant-current phase; all these works appear to rely on the popular MIT database provided by the authors of [29].

However, enhancing the robustness of the SOH estimation algorithm over completely different fast-charging profiles characterized by different charging phases has rarely been explored. The authors of [30] test their estimation algorithm on the MIT dataset with newly collected data on a different MSCC profile, whereas the authors of [31] combined the MIT dataset with data collected on CC–CV charging profiles. Both works describe feature engineering methods that are adaptable to different charging protocols. However, both models are then trained with the data from the cells cycled with one charging protocol and tested on cells charged with the same protocol. Furthermore, only CC–CV and multi-stage profiles are considered, disregarding PC protocols.

In summary, several issues still exist in the existing research on the capacity estimation of LIBs for fast-charging applications. First, most existing health features are extracted from complete charging sequences. Second, the robustness of capacity estimation is rarely evaluated experimentally over different fast-charging protocols, i.e., CC–CV, MSCC, and PC protocols, characterized by different charging phases. Most existing methods are validated based on the charging profiles of CC–CV charging current or on one multi-phase charging protocol characterized by different C-rate and duration of each phase, and even these works train and test their model on the same charging protocol. Finally, the aging datasets used in previous works are mainly laboratory tests that do not mimic real-world driving scenarios and are not truly representative of the aging phenomena affecting batteries in EVs.

1.1. Article contributions

The main objective of this work is to develop a SOH estimation method that can be applied to completely different fast-charging protocols and partial charging events in EV real-world scenarios. Hence, this work investigates charging protocol-independent health features to be employed for SOH estimation.

The main contributions of this study can be summarized as follows:

- **Development of a SOH estimation method that applies to partial charging events and a variety of fast-charging protocols.** The main novelty of this method is the use of reformulated SOH features as inputs to a machine learning model to estimate the

SOH. Taking inspiration from health features formulated in previous works, particular care was devoted to deriving features that are applicable in real-world automotive applications, regardless of the charging protocol and working with partial charging events. Moreover, the features are analyzed based on their applicability in real-world scenarios, highlighting the requirements for their use. After assessing their correlation with SOH, the most effective features are selected through the Minimum Redundancy Maximum Relevance (MRMR) algorithm, and a linear regression model is used to estimate the SOH for cells characterized by different fast-charging protocols.

- **Analysis of the robustness of the method in the presence of state of charge (SOC) estimation errors.** Since some of the proposed SOH features are computed relying on SOC knowledge, which is not known but must be estimated in real-world applications, the SOH estimation is also carried out considering different SOC estimation errors for the feature extraction.
- **A new dataset.** The 4-cell dataset of [18,32], and [33] is further expanded in this work by including two additional cells. The proposed algorithm is tested on the new dataset which reproduces EV real-world driving scenarios characterized by different fast-charging protocols and discharging driving cycles of a plug-in hybrid electric vehicle. Therefore, the aging mechanisms affecting EV batteries' operation are realistically induced.

2. Methods

2.1. Battery aging dataset

Fast-charging profiles provide significant information about the aging status of a battery cell [34]. In this work, we considered four 3Ah Samsung 30T cells, plus two other cells tested posterior that will be available in the open data source [35] soon. The test is composed of five different charging profiles, represented in Fig. 1 and described in [18], claimed to impact the battery lifespan positively: constant current (CC) performed on two cells (Figs. 1a, 1b, 1g, and 1h), boost constant current (BC) (Figs. 1c and 1i), pulse boost protocol with 0.1s negative pulse (BCNP 0.1s) (Figs. 1d and 1j), pulse boost protocol with 1s negative pulse (BCNP 1s) (Figs. 1e and 1k), and pulse boost protocol with rest (BCR) (Figs. 1f and 1l). The two cells CC and CC2 are charged with the same constant current charging protocol using a C-rate of 6C in the constant current phase. It is worth noting that the rest and negative pulses for the BCR and BCNP 0.1s cells, respectively, are not visible from Fig. 1. This is because the battery's experimental data (including both charging and driving cycles) was recorded at a frequency of 1 Hz, which is too low to capture the short duration (0.1s) of the rest and negative pulses [32]. To clearly observe these pulses, the initial fast charging performed under the BCNP and BCR protocols was separately recorded in [32] at a high logging rate (50 Hz).

Each cell is charged with the respective charging profile from 10% SOC to 80% SOC using the same mean current (C-rate of 2.8C). The fast charge occurs before the cell reaches the maximum voltage of 4.2 V; then, the constant voltage (CV) charging mode is activated to avoid damage to the battery. After each charging phase, the cell is depleted back to 10% SOC using repeated drive cycles.

As the cells age, the charging time needed to reach the designed SOC, i.e., 80%, is reduced due to the lower cell capacity. In later aging stages, this trend is inverted for some cells due to the longer CV charging phase, where the current is reduced to avoid the overvoltage condition. Indeed, the upper voltage limit of 4.2 V is reached faster as the cells age due to the lower cell capacity and higher internal resistance. The information on the charging profiles is used to formulate some of the SOH features presented in the next section.

Table 1
SOH features and symbols.

SOH features	Symbol
Constant current charging time	$t_{\mathrm{CC,norm}}$
Constant voltage charging time	t_{CV}
SOC at CC/CV transition	$SOC_{\mathrm{CC-CV}}$
Voltage slope at the beginning of CC charging	$\frac{dV}{dt}_{\mathrm{in,CC,norm}}$
Voltage slope at the end of CC charging	$\frac{dV}{dt}_{\mathrm{end,CC,norm}}$
Average voltage over constant current charging	$V_{\mathrm{av,norm}}$
Ah throughput	
Mileage	
Mean temperature during charging	

2.2. SOH features

To develop an accurate and practical estimation model, the features of the model must be carefully selected. One of the main objectives of this work is to identify the features that are most correlated with SOH and exhibit good robustness across different fast-charging profiles for EV applications; furthermore, particular care was placed on the practical availability of these features in a real operating scenario.

In this section, the nine SOH features investigated in this work are presented and reported in Table 1. Of these nine features, seven are extracted from a single charging phase. As discussed in the Introduction, these features are expected to be very reliable in predicting SOH because they are evaluated under the relatively repeatable conditions of the charging phases with respect to the driving phases. In addition to these, two cumulative features that are very commonly considered for SOH estimation were also included in our analysis: the vehicle mileage and the Ah throughput, evaluated over the entire vehicle lifetime. Note that, for ease of notation, we used the subscript $_{\mathrm{CC}}$ to denote the charging phase that precedes the CV phase for all the charging protocols, whether this phase is indeed a constant current phase or not.

2.2.1. Constant current charging time $t_{\mathrm{CC,norm}}$

The constant current charging time $t_{\mathrm{CC,norm}}$ represents the time required to charge the battery from an initial state of charge SOC^* to a final voltage V^*, divided by the corresponding charging time for a fresh cell. Mathematically, $t_{\mathrm{CC,norm}}$ can be written as follows:

$$t_{\mathrm{CC,norm}} = \frac{t_{\mathrm{CC}}}{t_{\mathrm{CC,fresh}}} \tag{1}$$

$$t_{\mathrm{CC}} = t(SOC = SOC^*) - t(V = V^*) \tag{2}$$

where $t_{\mathrm{CC,fresh}}$ is the value of t_{CC} that was measured for a fresh cell and SOC^* and V^* are tuning parameters for this feature. Fig. 2 provides a graphical representation of how to compute the $t_{\mathrm{CC,norm}}$ for an aged cell[1] over one specific charging profile depicted in black. First, the time t_{CC} intercurring between the SOC^* (blue points in the figure) and the V^* (red points) is measured for the aged cell; then, using the first charging cycle of the same cell (depicted in gray), the $t_{\mathrm{CC,fresh}}$ is computed. Finally, the time is normalized through (1) to obtain $t_{\mathrm{CC,norm}}$. Through this formulation, the feature can be computed for partial constant current charging profiles that start with an $SOC < SOC^*$ and end with a voltage $V > V^*$, where $SOC^* < SOC(V = V^*)$: hence, the whole charging curve is not needed to obtain the feature. It is worth specifying that the charging segment length must be selected to satisfy the requirement $SOC^* < SOC(V = V^*)$.

This is similar to other features found in the literature, where the time needed to raise the battery voltage from a starting value to a final value is used instead [31,36]; that feature was reported to be a powerful SOH feature, highly correlated with capacity fading. However, that formulation was found to be ineffective with our dataset, as shown

[1] In this case, we consider the BC cell, but the procedure is the same also for the other charging profiles.

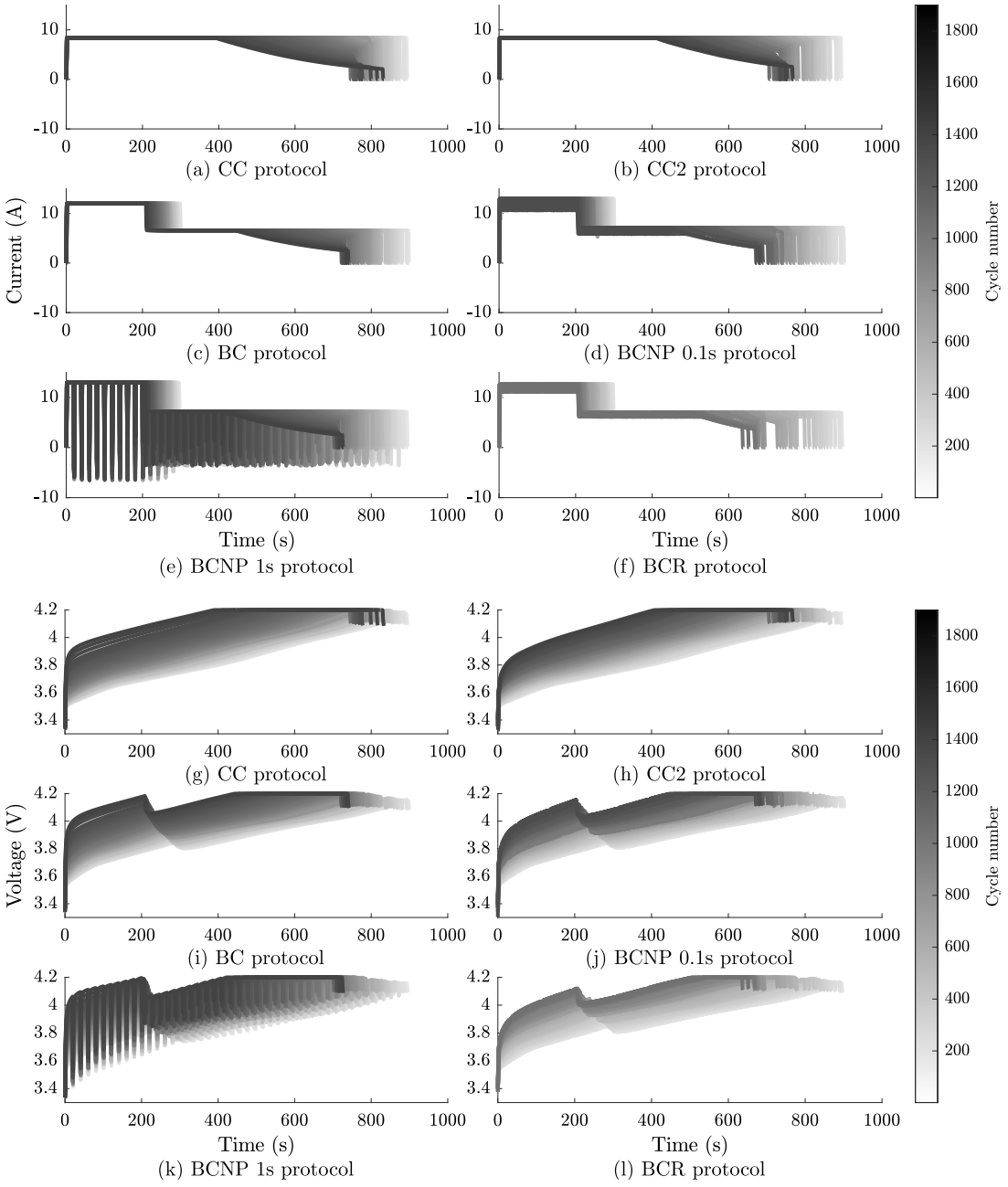

Fig. 1. Charging current and voltage profiles for all cells. Current profiles for protocols (a): constant current; (b): constant current 2; (c): boost constant current; (d) pulse boost with 0.1s negative pulse; (e) pulse boost with 1s negative pulse; (f) pulse boost with rest. Voltage profiles for protocols (g): constant current; (h): constant current; (i): boost constant current; (j) pulse boost with 0.1s negative pulse; (k) pulse boost with 1s negative pulse; (l) pulse boost with rest.

by the results in the Supplementary material. Fig. S1a, Fig. S1b, and Fig. S1c show that the time of constant current charging computed through the formulation of [31,36] from a minimum voltage of 3.6 V, 3.8 V, and 3.9 V, respectively, becomes less correlated with the SOH as the minimum voltage increases. On the other hand, the time of constant current charging computed through our formulation shows a higher correlation with SOH for SOC^* values of 11%, 20%, and 30%, as shown in Fig. S2a, Fig. S2b, and Fig. S2c, respectively.

Working with our dataset, we found that the formulation of the feature proposed in [31,36] has a strong correlation with SOH only if the considered period includes at least part of the early, steeper portion of the voltage curve. Therefore, a low initial voltage threshold should be selected to obtain good results. However, this is potentially misleading because the very first part of the charging phase could be included as well. At the very beginning of the charging phase, the voltage values are greatly influenced by the internal resistance, which is highly dependent on SOC. Therefore, this feature is only effective if the charging sequences always start at the same SOC; in other words, the feature does not adapt to partial charging events. To work around this problem, we replaced the initial voltage threshold with an initial SOC threshold; in this way, the initial threshold is not dependent on the internal resistance.

The formulation of the charging time proposed in this work was developed to eliminate its dependence on the SOC value at the beginning of charging. Moreover, to increase the robustness of this feature with respect to different C-rates, t_{CC} was normalized with respect to the feature computed for the fresh cell $t_{CC,fresh}$, as shown in Eq. (1); without this normalization, different C-rates would produce largely different values for t_{CC}.

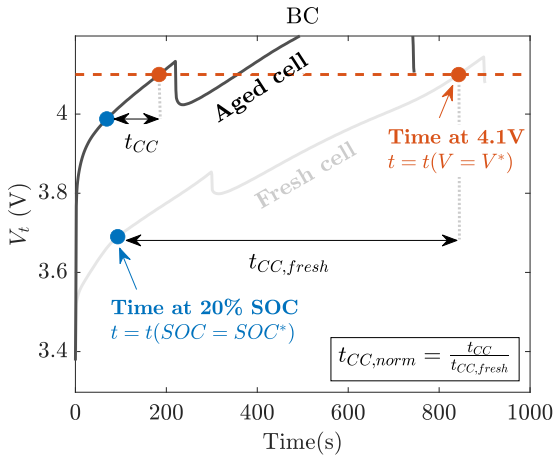

Fig. 2. Voltage profiles of the fresh (light gray) and aged (dark gray) BC cell. The red line is the value of V^*. (For interpretation of the references to color in this figure legend, the reader is referred to the web version of this article.)

For all cells, $t_{\mathrm{CC,norm}}$ tends to decrease as the cell ages due to the lower cell capacity. Moreover, a very high correlation between the feature and SOH is visible in the first subplot of Fig. 3a for all the battery cells, showing its effectiveness. Fig. 3 shows the feature obtained with $SOC^* = 20\%$ and $V^* = 4.1$ V.

2.2.2. Constant voltage charging time t_{CV}

The duration of the constant voltage charging phase until a final SOC value is reached SOC_{**}. As the cell ages, its ohmic resistance undergoes a significant increase, leading to higher voltage values given the same current and SOC. As a consequence, the upper voltage limit is reached earlier, leading to the activation of CV charging mode and an increase in the value of the t_{CV} feature [37]. The results shown in Fig. 3b are calculated considering $SOC_{**} = 80\%$. It should be noted that, contrary to t_{CC}, this feature cannot be normalized with respect to the fresh cell value due to the null value of the feature for the fresh cell.

2.2.3. SOC at CC/CV transition $SOC_{\mathrm{CC-CV}}$

The SOC value is observed at the transition from the constant current to the constant voltage phase. Due to the higher internal resistance and lower capacity, $SOC_{\mathrm{CC-CV}}$ decreases as the cell ages, as shown in Fig. 3c. Unfortunately, this novel feature did not prove to show a strong correlation with SOH for our dataset; furthermore, it could be highly susceptible to errors in SOC estimation.

2.2.4. Voltage slope at the beginning of CC charging $\frac{dV}{dt}_{\mathrm{in,CC,norm}}$

The slope of the voltage curve at the beginning of charging. At the beginning of charging, the battery voltage rises very quickly due to the increase in ohmic voltage. Hence, $\frac{dV}{dt}_{\mathrm{in,CC}}$ indirectly quantifies the internal resistance at the beginning of the charging phase. In this work, the application of this feature, originally proposed in [37], is extended to fast-charging and different C-rates thanks to the following formulation:

$$\frac{dV}{dt}_{\mathrm{in,CC}} = \frac{\Delta V}{\Delta t} \tag{3}$$

$$\Delta t = \Delta t_{\mathrm{in},0} \cdot \frac{I_{2.8C}}{I_{mean}} \tag{4}$$

$$\frac{dV}{dt}_{\mathrm{in,CC,norm}} = \frac{\frac{dV}{dt}_{\mathrm{in,CC}}}{\frac{dV}{dt}_{\mathrm{in,CC,fresh}}} \tag{5}$$

where ΔV is the voltage increase experienced over the corrected time step Δt. This corrected time step was deemed necessary to guarantee the robustness of the feature with respect to different current profiles. In essence, it is a normalization of a fixed time step $\Delta t_{\mathrm{in},0}$ with respect to the mean measured current I_{mean}; $I_{2.8C}$ instead is a constant parameter corresponding to a nominal discharge current at 2.8C.

Moreover, the slope at the beginning is normalized to the slope obtained with the fresh cell $\frac{dV}{dt}_{\mathrm{in,CC,fresh}}$. In Fig. 3d, the results show the $\frac{dV}{dt}_{\mathrm{in,CC,norm}}$ computed with $\Delta t_{\mathrm{in},0} = 10$ s. The main limitation of this feature is that it can be used only when the charging phase starts from the same SOC, due to the dependence of the ohmic resistance from SOC.

2.2.5. Voltage slope at the end of CC charging $\frac{dV}{dt}_{\mathrm{end,CC,norm}}$

The slope of the voltage curve at the end of the charging phase preceding the CV phase. The $\frac{dV}{dt}_{\mathrm{end,CC}}$ feature overcomes the limit of the previous one since it is not dependent on the SOC at the beginning of the charging event. The following formulation was adopted to compute the feature:

$$\frac{dV}{dt}_{\mathrm{end,CC}} = \frac{\Delta V}{\Delta t} \tag{6}$$

$$\Delta t = \Delta t_{\mathrm{end},0} \cdot \frac{I_{2.8C}}{I_{mean}} \tag{7}$$

$$\frac{dV}{dt}_{\mathrm{end,CC,norm}} = \frac{\frac{dV}{dt}_{\mathrm{end,CC}}}{\frac{dV}{dt}_{\mathrm{end,CC,fresh}}} \tag{8}$$

Although in [37] a high correlation with SOH was reported when using low current charging profiles, this feature appears to lose its efficacy in fast-charging applications as shown in Fig. 3e, where it is computed considering $\Delta t_{\mathrm{end},0} = 400$ s.

2.2.6. Average voltage over constant current charging $V_{\mathrm{av,norm}}$

The average voltage observed between an initial SOC SOC^* and a final voltage value V^*. As a descriptive statistic of the voltage charging curve [34], V_{av} increases along with cell aging due to the higher internal resistance. Also, in this case, the feature is normalized with respect to the fresh cell value $V_{\mathrm{av,fresh}}$ as follows:

$$V_{\mathrm{av,norm}} = \frac{V_{\mathrm{av}}}{V_{\mathrm{av,fresh}}} \tag{9}$$

The normalized average voltage $V_{\mathrm{av,norm}}$ exhibits a strong correlation with capacity fading across various charging protocols, as shown in Fig. 3f, competing closely with the normalized charging time $t_{\mathrm{CC,norm}}$ for the title of the best SOH feature.

2.2.7. Ah throughput

The total capacity that the battery delivers or stores. Ah throughput is a cumulative SOH feature that is computed by Coulomb counting, i.e., by integrating the absolute value of cell current over time, and has been widely used as a SOH feature [38]. However, this cannot always be measured reliably in an EV; a single fault occurrence in the BMS or current sensors throughout the whole vehicle lifetime, if not repaired immediately, could alter its value in an unrecoverable manner. The high correlation between this feature and SOH is clearly shown in Fig. 3g.

2.2.8. Mileage

Distance traveled by the vehicle. Generally, battery life is represented by the number of cycles, which is deeply connected with battery aging. However, in actual usage of an EV, the equivalent full cycle number does not have much practical significance and convenience for measuring the health of the battery pack; instead, mileage can be used as a substitute measure of cycle number, with a similar meaning of Ah throughput [39]. In this work, Ah throughput and mileage have the same trend over the battery lifetime due to the periodicity of the driving cycles discharging profiles, as shown in Figs. 3g and 3h.

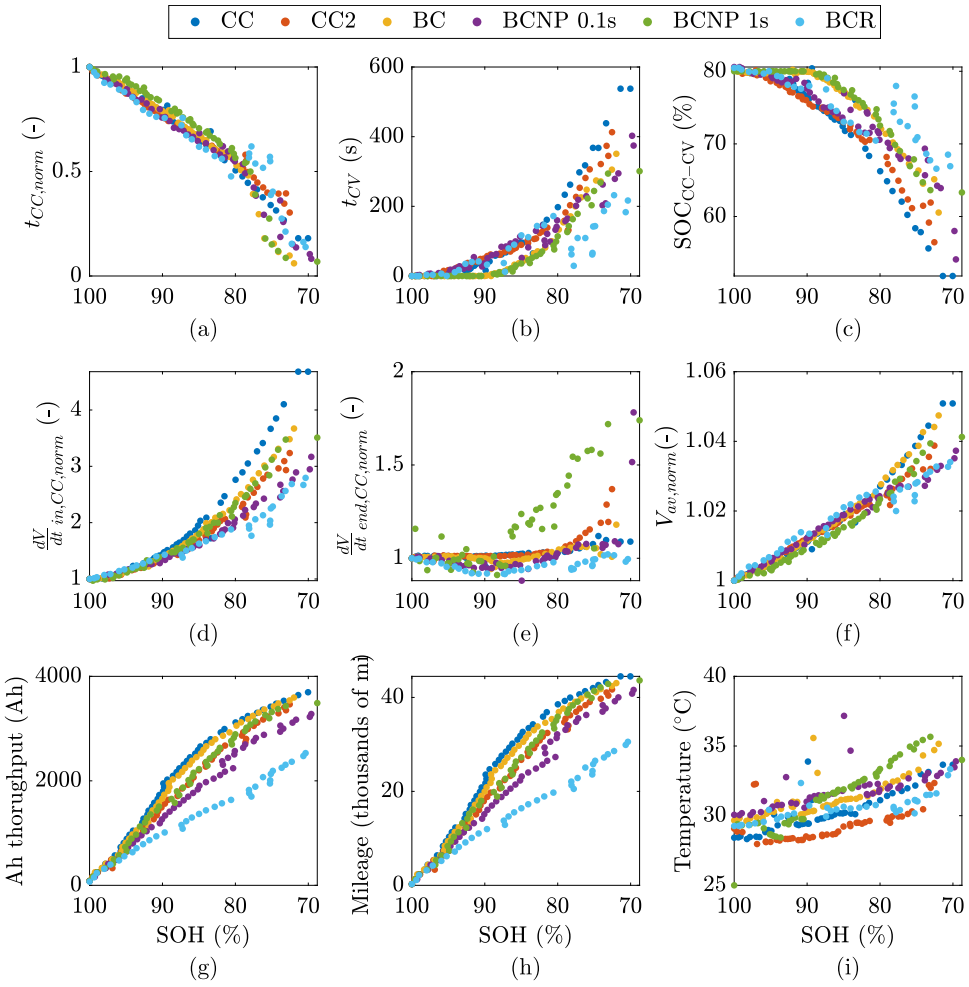

Fig. 3. Values of the SOH features computed for all the tested charging profiles, represented as a function of SOH. (a): constant current charging time $t_{CC,norm}$. (b): constant voltage charging time t_{CV}. (c): SOC at CC/CV transition SOC_{CC-CV}. (d): voltage slope at the beginning of CC charging $\frac{dV}{dt}_{in,CC,norm}$. (e): voltage slope at the end of CC charging $\frac{dV}{dt}_{end,CC,norm}$. (f): average voltage over constant current charging $V_{av,norm}$. (g): Ah throughput. (h): Mileage. (i): mean temperature during charging.

2.2.9. Mean temperature during charging

The mean temperature over a single charging procedure. As the cell ages, the battery Joule losses increase, given the same charging profile, leading to higher cell temperatures. Therefore, the mean temperature over a charging procedure exhibits an increasing trend, given the same environment temperature, as shown in Fig. 3i. Real-life applicability of this feature is limited by the fact that its behavior is related to ambient temperature.

To map the relationship between mileage and SOH, extensive data is needed. Since collecting this data from real-world vehicles is too time-consuming, a more practical approach is to use a high-fidelity vehicle model to generate realistic battery current profiles. Relying on these current profiles, much shorter lab experiments based on realistic driving conditions can be carried out. This latter approach is the one used to generate the dataset in this paper.

3. Results and discussion

3.1. Analysis of the features

3.1.1. Practical considerations

As mentioned in the previous section, every feature has its limitations and most of them cannot be computed in every possible charging condition. Indeed, a few requirements must be met to correctly compute each feature, as summarized in Table 2.

For example, the $\frac{dV}{dt}_{in,CC,norm}$ feature, due to the dependence of the internal resistance with SOC, depends on the SOC at the beginning of the charging phase. Therefore, an SOH estimation model using this feature must trained with charging sequences having the same initial SOC, and can then only be used if a charging sequence starts at that same SOC. This requirement is particularly restrictive in real-world scenarios since the user can charge the battery starting from very different SOC values.

On the other hand, the other requirements are more easily satisfied in real-world conditions: due to the high C-rate of fast-charging profiles, the charging CV mode is usually activated during charging; SOC needs to be generally estimated by BMS to predict the vehicle range; SOC^*, V^*, and SOC_{**} can be selected so as to cover a wide range of charging events based on the expected driver behavior.

3.1.2. Correlation analysis

A regression analysis was carried out to assess the correlation between the previously introduced SOH features and SOH, providing some important indications of the most effective features that need to be selected as inputs of the estimation model. The Pearson correlation coefficient was used to quantify the correlation between SOH features and SOH. Pearson correlation analysis is typically adopted in statistics to measure the degree of correlation between two variables. The Pearson correlation coefficient $p_{x,y}$ is calculated as the quotient of the

Table 2
Requirements needed for the features to be computed and used in an SOH estimation model.

SOH features	Requirements				
	Charging starts from the same SOC	Charging does not start in CV mode and voltage reaches upper limit	SOC is known or estimated	Charging starts with $SOC \leq SOC^{*}$ and ends with $V \geq V^{*}$	Charging ends with $SOC \geq SOC_{**}$
$t_{CC,norm}$			✓	✓	
t_{CV}		✓			✓
SOC_{CC-CV}		✓	✓		
$\frac{dV}{dt}_{in,CC,norm}$	✓		✓		
$\frac{dV}{dt}_{end,CC,norm}$		✓			
$V_{av,norm}$			✓	✓	
Ah throughput					
Mileage					
Mean temperature during charging					

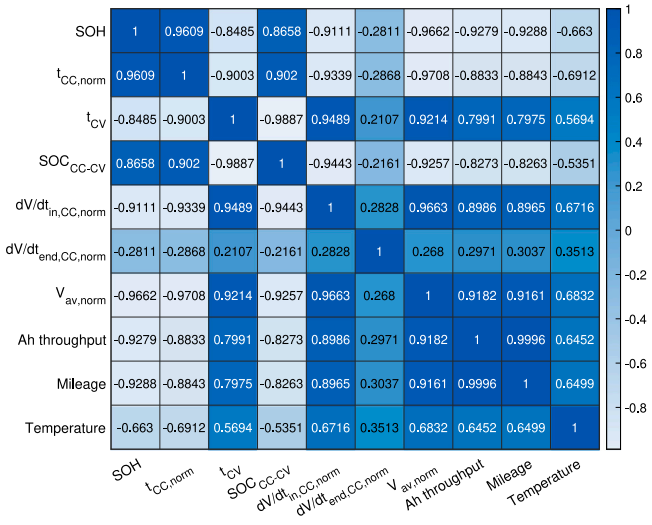

Fig. 4. Pearson coefficients for all the SOH features.

covariance and standard deviation between the input variables x and a response variable y:

$$p_{x,y} = \frac{\mathrm{cov}(x,y)}{\sigma_x \sigma_y} \tag{10}$$

where $\mathrm{cov}(x,y)$ is the covariance of x and y, while σ_x and σ_y are the standard deviation of x and y, respectively. The Pearson coefficient can range between −1 and 1, and the closer the absolute value of the correlation coefficient is to 1, the stronger the correlation is. While positive values represent a positive correlation, negative values represent a negative correlation.

Using all features derived from the raw data as input for the SOH estimation model can result in a decrease in accuracy due to the presence of erroneous data or overfitting. Therefore, outliers[2] were removed before performing the analysis.

The results of the correlation analysis are shown in Fig. 4. All features exhibit a strong linear correlation with SOH, as evidenced by Pearson coefficients with absolute values exceeding 0.85. The only exceptions are the final slope $\frac{dV}{dt}_{end,CC,norm}$ and mean temperature with coefficients equal to −0.28 and −0.66, respectively. As expected from the graphical results of Fig. 3, the most highly correlated features are the constant current charging time and the average voltage. It is worth noting that, in our tests, the normalization of these features with respect to the fresh cell is necessary to obtain a high correlation with SOH in the different fast-charging profiles.

The normalization of the different features with respect to the fresh cell enhances the robustness of the features against the different charging protocols. Indeed, the voltage slope at the beginning of CC charging $\frac{dV}{dt}_{in,CC}$, and the average voltage V_{av} have a significantly lower correlation than their normalized version. The Pearson coefficient for the $\frac{dV}{dt}_{in,CC}$ go from −0.76 to −0.91 for $\frac{dV}{dt}_{in,CC,norm}$; the Pearson coefficients for the V_{av} go from −0.88 to −0.96 for $V_{av,norm}$. On the other hand, the normalization of the time of constant current charging and the voltage slope at the end of CC charging do not provide particular advantages in terms of correlation for this particular dataset. However, this approach could be beneficial for other datasets.

3.1.3. Feature selection

Instead of using all available feature variables in the data, only a subset of features was selected to be used in the estimation model. Feature selection leads to several advantages, i.e., reduction of the computational cost, and improvement of the regression accuracy. Moreover, using fewer features also requires less training data.

In this work, feature selection was carried out through the Minimum Redundancy Maximum Relevance (MRMR) algorithm [40]. The MRMR relies on the concept of mutual information of two variables, ranking the features to minimize the redundancy of the feature set and maximize the relevance of the feature set to the response variable. The mutual information I of the input x and response y variables is defined based on their joint probabilistic distribution $p(x,y)$ and the respective marginal probabilities $p(x)$ and $p(y)$:

$$I(x,y) = \sum_{i,j} p(x = x_i, y = y_j) \log\left(\frac{p(x = x_i, y = y_j)}{p(x = x_i) \cdot p(y = y_j)}\right) \tag{11}$$

Since the mutual information quantifies the similarity between the two variables, the idea of minimum redundancy is to select the features that are mutually maximally dissimilar, leading to a better representation of the entire dataset. The minimum redundancy condition is achieved through the minimization of W_S, defined as follows:

$$W_S = \frac{1}{|S|} \sum_{x,z \in S} I(x,z) \tag{12}$$

where S denotes the subset of features, and $|S|$ is the number of features in S. Once again, mutual information is used to quantify the relevance of S with respect to the response variable y. Hence, the maximum relevance condition is satisfied by maximizing the value of V_S, which is defined as:

$$V_S = \frac{1}{|S|} \sum_{x \in S} I(x,y) \tag{13}$$

The MRMR feature set is obtained by optimizing the conditions in Eqs. (12) and (13), simultaneously. To achieve this goal, the features

[2] The outliers were defined as elements different more than three standard deviations from the mean value.

are ranked based on their mutual information quotient (MIQ) value which, for feature x, is computed as:

$$\mathrm{MIQ}_x = \frac{V_x}{W_x} = \frac{I(x,y)}{\frac{1}{|S|}\sum_{z\in S} I(x,z)} \tag{14}$$

MRMR ranks all the features in ascending order according to their MIQ. The features were ranked by the MRMR as follows:

1. $t_{\mathrm{CC,norm}}$,
2. Mileage,
3. $SOC_{\mathrm{CC-CV}}$,
4. $V_{\mathrm{av,norm}}$,
5. $\frac{dV}{dt}_{\mathrm{in,CC,norm}}$,
6. t_{CV},
7. $\frac{dV}{dt}_{\mathrm{end,CC,norm}}$,
8. Ah throughput,
9. Temperature.

By the correlation analysis, $t_{\mathrm{CC,norm}}$ emerges as the best feature. However, as shown in the ranking, the MRMR enables drawing different conclusions from the simpler correlation analysis based on Pearson coefficients. Indeed, powerful features with high Pearson coefficients, such as $V_{\mathrm{av,norm}}$ and Ah throughput, are placed in lower ranks. This is because they also have a high mutual correlation with $t_{\mathrm{CC,norm}}$ and Mileage, respectively. In other words, if a model is trained using $t_{\mathrm{CC,norm}}$ and mileage as features, then adding $V_{\mathrm{av,norm}}$ does not add significant information that was not already captured by $t_{\mathrm{CC,norm}}$ and mileage.

3.2. Application of the features to an SOH estimation model

The main workflow of our SOH estimation algorithm is depicted in Fig. 5. During the charging phase, the time, current, voltage, SOC, and temperature signals are recorded. Then, once the charging phase ends, each SOH feature is extracted, provided that the phase meets the corresponding requirements summarized in Table 2. It is worth noting that the computation of these SOH features is straightforward and computationally light for any BMS. Afterward, the most effective features are selected as inputs to the linear regression model; finally, the linear regression model is used to estimate the SOH.

3.2.1. Linear regression model(s)

Due to its low computational complexity and its easy implementability in vehicle BMS, we selected the linear regression model as the SOH estimation model to exploit the high linear correlation between SOH features and SOH. Moreover, compared to more complex ML algorithms, the linear regression model is characterized by few tuning parameters and can better generalize with a small number of training samples. Therefore, since our dataset is made of only six cells, the linear regression model seems the most appropriate solution. However, it is worth specifying that, if the linear correlation between the features and capacity fade was weaker, more complex machine learning algorithms could be used instead of linear regression to map the non-linear relationship between the features and SOH.

In order to test the effectiveness of the SOH features discussed so far, we developed four SOH estimation models using linear regression; these four different models differ in the number of features that were considered, ranging from one to four. The exact features to be used were selected based on the feature importance ranking discussed in the previous section.

To evaluate their robustness with respect to different fast-charging protocols, the models were trained using the experimental data from two protocols (CC and BCNP 0.1s) and tested on the remaining four protocols (CC2, BC, BCNP 1s, and BCR), as reported in Table 3. The parameters of the linear regression models were obtained using the least square method through the MATLAB function *fitlm* [41]. The

Table 3
Training and testing cells for the linear regression model.

Battery cell	Charging protocol	Number of total cycles	Training or testing
CC	Constant current charging (2.8C)	1908	Training
CC2	Constant current charging	1876	Testing
BC	Boost constant current	1908	Testing
BCNP 0.1s	Pulse boost protocol with 0.1s negative pulse	1730	Training
BCNP 1s	Pulse boost protocol with 1s negative pulse	1876	Testing
BCR	Pulse boost protocol with rest	1876	Testing

estimates and the estimation error obtained with the trained models on the test data are shown in Figs. 6a, 6b, 6c, and 6d using different set of features for the CC2, BC, BCNP 1s, and BCR cells, respectively, and in Fig. 7.

Overall, all models reach reasonable accuracy, with the estimation error always remaining well below 10%. Another conclusion that appears to hold true for all protocols is that a significant improvement in accuracy can be obtained by using two features, whereas additional features produce only minor improvements. Protocol BCR exhibits a somewhat more complex behavior, as the model with one feature appears to be more accurate in starting from a SOH of approximately 90%. This seems to be coincidental: the model underestimates the state of health of the fresh cell and then underestimates the rate of aging, which produces the illusion of better accuracy with a moderately aged cell as the two errors balance each other.

Furthermore, some notable differences are visible between the different charge protocols and between the early aging phase and the end-of-life. As long as the SOH remains above 80%, the estimation error of all models remains below 5%. If we restrict our attention to the models with at least two features, this error is even smaller and is always below 3.5%, and all these models exhibit consistent error patterns with a general tendency to overestimate SOH. When SOH drops below 80%, however, the models exhibit a more erratic behavior. Again considering only the models with at least two features, the models remain consistent among themselves in their estimations but significantly lose their accuracy with respect to the test data. For the CC2 protocol, the models still show a somewhat regular tendency to overestimate SOH; they are however unable to predict the two dips that can be seen in the experimental profile. For the BC and BCNP 1s, on the other hand, the models predict a sharp increase in the rate of aging which is not visible in the real SOH profile; in general, the highest estimation errors are seen for SOH below 80%. Differently from the previous range, the models underestimate rather than underestimate the SOH. Finally, when tested on the BCR protocol, the models predict an unlikely increase in the SOH. This situation (BCR protocol, SOH below 80%) is where the absolute worst accuracy is achieved, with estimation errors as high as 9% due to a significant overestimation of the SOH.

In summary, a significant degradation in the model performance was observed for all models when considering the boost charging profiles (i.e. BC, BCNP 1s, and BCR) after the state of health decreased below 80%. For practical applications, this may not be a major issue as this value is the threshold that is typically considered as the end-of-life for automotive applications. Nonetheless, it is important to assess the underlying causes. First, all models show this behavior regardless of the number of features; this suggests the feature that is common to all models, $t_{\mathrm{CC,norm}}$, is responsible. The reason was found to be in the way this value is calculated for the boost charging profiles, which may be susceptible to an irregular pattern after a certain SOH threshold; Fig. 2

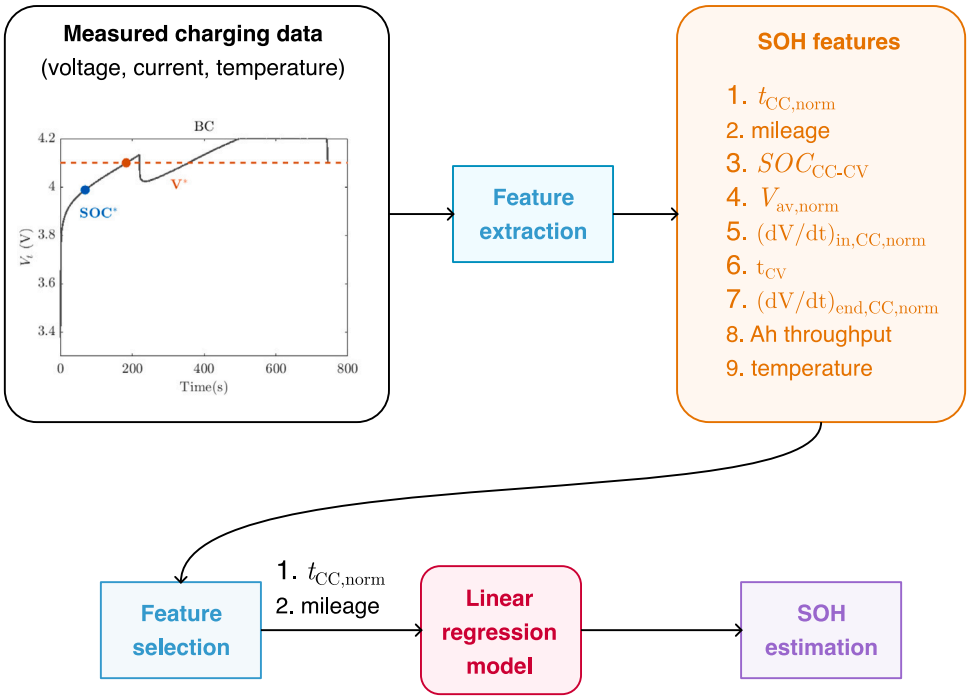

Fig. 5. SOH estimation workflow.

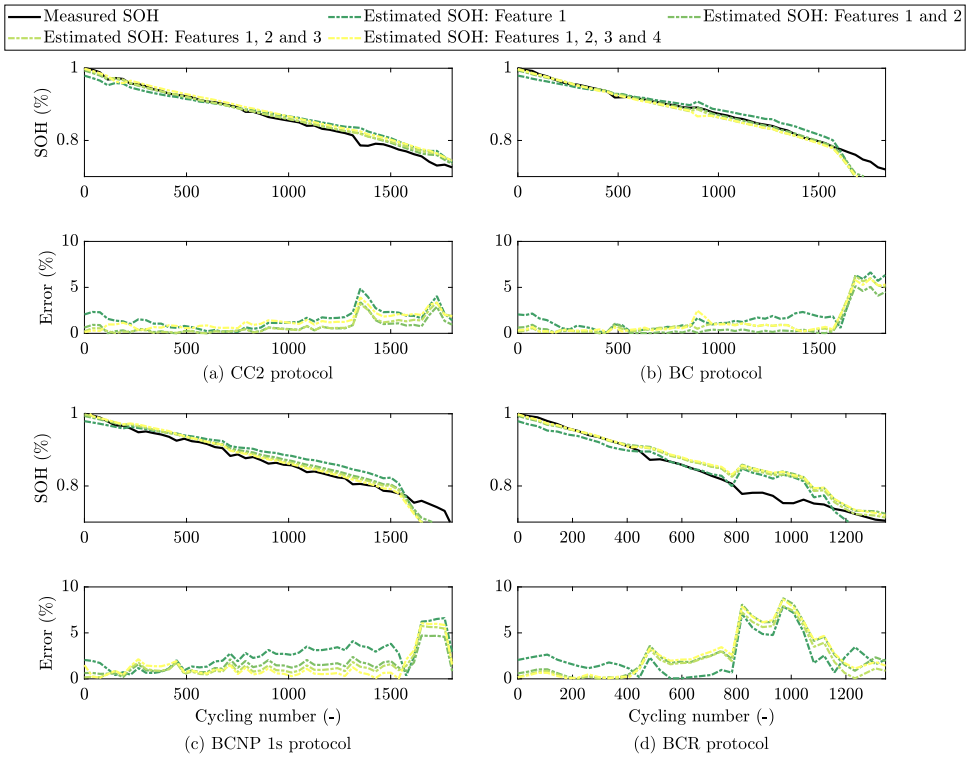

Fig. 6. SOH estimation results using different sets of features on the testing cells(a): constant current 2, (b): boost constant current, (c) pulse boost with 1s negative pulse, and (d): pulse boost with rest.

helps to illustrate the issue as it manifests for the BC protocol. For a relatively new cell, the value of V^* is reached during the second CC phase with a lower current. As the cell ages, the time at which V^* is reached decreases smoothly. Under a certain SOH threshold, however, the highest voltage reached in the first CC phase reaches and exceeds V^*; from this moment on, V^* will be first encountered in the first CC phase. Furthermore, this transition causes a sharp change in the $t_{CC,norm}$ feature, which is not due to an actual (significant) change of the SOH.

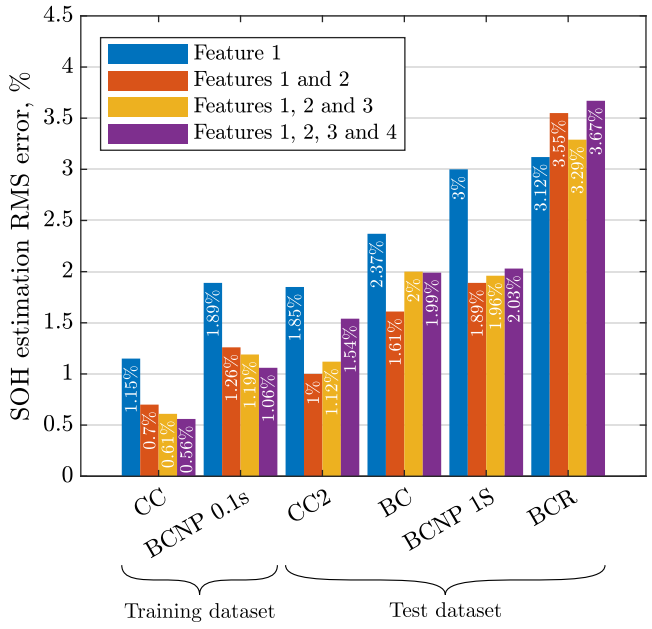

Fig. 7. SOH estimation results on the testing cells using different sets of features.

In practice, this phenomenon was observed at around 80% SOH, which is consistent with the previously observed loss in accuracy.

In conclusion of the feature analysis, the two best features, i.e., $t_{\mathrm{CC,norm}}$ and mileage, should be selected as inputs to the linear regression model.

To prove the applicability of the estimation method to different portions of the charging curve, the effectiveness of the SOH estimation was assessed when computing the $t_{CC,norm}$ feature for different SOC^* and V^* values. As shown in Table 4, the RMSE of the SOH estimation does not significantly change for the different SOC^* and V^*, proving the indicator to be robust against partial charging. Indeed, the length of the charging segment does not appear to affect the results in a consistent manner: we cannot conclude that longer charging segments lead to more accurate estimates, or vice versa. It is worth noting that the missing values in the table correspond to tests where the SOC at V^* is greater than the SOC^* at least for one charging phase. Indeed, the feature cannot be computed for all the combinations of V^* and SOC^*.

3.2.2. Robustness to SOC error

The results in the previous section assumed perfect knowledge of the battery's state of charge, which was obtained by Coulomb counting. Although Coulomb counting is reliable in laboratory conditions, its effectiveness is hindered in real applications due to different factors [42], e.g., lower sensor accuracy. In real operation, the SOC is provided by the SOC estimation algorithm, which is of course inherently subject to its own estimation error. This error has an impact on the SOH estimation models introduced in the previous section. For example, $t_{\mathrm{CC,norm}}$, which was used by all models, relies on knowledge of the SOC.

For this reason, an assessment of the SOH estimation models with respect to errors in the SOC estimates was deemed appropriate. For this analysis, we restricted our attention to the model that was deemed more promising when trading off accuracy and complexity, i.e. the model using two features ($t_{\mathrm{CC,norm}}$ and mileage). The previous tests were repeated while artificially introducing an offset error in the SOC ranging from −5% to 5%, as shown in Figs. 8a, 8b, 8c, and 8d for the CC2, BC, BCNP 1s, and BCR cells, respectively.

Table 5 shows the root mean square value of the estimation error for each charging protocol, with different values of the injected SOC error. As expected, the estimation accuracy is indeed affected by the presence of an error in the SOC; nevertheless, the accuracy of the model remains satisfying. Furthermore, injecting an SOC error produces consistent errors in the SOH estimation, without altering the overall prediction trends of the model. This is clearly visible in Fig. 8, which shows the SOH predictions and estimation errors that were thus obtained on the test charging protocols. This robustness is likely attributable to the use of the mileage, which is not affected by the SOC error, as the second input feature. Moreover, the simplicity of linear regression over other data-driven algorithms allows one to obtain accurate results, avoiding the tendency towards over-fitting typical of other more complex machine learning models.

4. Conclusion

Prior works have demonstrated the effectiveness of data-driven SOH estimation methods when exploiting SOH features that can be easily calculated during charging events. However, these studies are limited in their practical applicability as they fail to account for the wide variability that can be experienced in real-world operation, focusing instead on full charging events in a lab environment. Moreover, few studies consider fast-charging events and different charging protocols. In this study, we investigated nine SOH features, some of which are based on novel formulations that we modified to improve their flexibility for different charging events, and developed a linear regression model to test them using a dataset that includes six different fast-charging protocols.

We found that a linear regression model, which combines one feature extracted from the charging profile ($t_{\mathrm{CC,norm}}$) and one easily available cumulative feature (the vehicle's mileage), achieves reasonable accuracy when tested on fast-charging protocols that are different from the training protocols. We also found that, owing to its simple and interpretable structure, the linear regression model is also robust with respect to errors in SOC estimation (which affects the $t_{\mathrm{CC,norm}}$ feature). The study also discusses the relative importance of the nine SOH features based on the results of a correlation and a feature importance analysis.

Our results suggest that exploiting charging events is in fact a practical approach to monitor the SOH of an EV battery pack, even when considering fast-charging and different charging protocols; our work also provides some novel SOH features[3] that can be effectively evaluated and used even for partial charging events, which are very common in real-world operation.

Nonetheless, this work can be improved in different aspects in future research. Even if the proposed features are flexible to a wide range of charging events, they are still not applicable to all charging situations; nonetheless, different features might complement each other. Future work could therefore focus on developing two or more separate SOH estimation models with different features. After a charging event is completed, the prediction of the model for which the most reliable features were available could be selected. Furthermore, we acknowledge that, at present, fast charging is only a limited portion of the whole battery usage time, although this is expected to grow with the development of EV charging infrastructures. Nevertheless, the method proposed in this work can complement other SOH estimation algorithms based on the more common slow charging. Indeed, by integrating SOH estimations from different methods across various charging/discharging phases, a more accurate and reliable SOH estimation could be achieved. Moreover, the estimation method has not been tested over the realistic scenario where different charging protocols occur randomly throughout the battery's lifetime, due to the lack of experimental data. Nonetheless, the estimation method should be able to provide accurate results even for such a complex scenario. Once the aging campaign (or vehicle usage) begins, it is crucial to identify the charging protocol used for each charging phase and normalize the health features with respect to the feature value obtained for the fresh cell cycled with the corresponding protocol.

[3] or rather, novel formulations of commonly used features.

Table 4
Root mean square error of the SOH estimation using time of constant current charging and mileage as inputs to the linear regression model, using different values of SOC^* and V^* to define the time of constant current charging.

Protocol	V^*	SOC^*	RMSE, %
CC2	4.0 V (≈ 15%–60%)	10%	1.62
		20%	–
		30%	–
	4.05 V (≈ 20%–70%)	10%	1.38
		20%	1.35
		30%	–
	4.1 V (≈ 30%–75%)	10%	1.51
		20%	1.47
		30%	1.35
	4.15 V (≈ 35%–80%)	10%	1.35
		20%	1.31
		30%	1.19
BC	4.0 V (≈ 15%–60%)	10%	1.48
		20%	–
		30%	–
	4.05 V (≈ 20%–70%)	10%	1.38
		20%	1.35
		30%	–
	4.1 V (≈ 30%–75%)	10%	1.51
		20%	1.47
		30%	1.35
	4.15 V (≈ 35%–80%)	10%	1.35
		20%	1.31
		30%	1.19
BCNP 1s	4.0 V (≈ 15%–60%)	10%	1.62
		20%	–
		30%	–
	4.05 V (≈ 20%–70%)	10%	1.73
		20%	1.79
		30%	–
	4.1 V (≈ 30%–75%)	10%	1.78
		20%	1.87
		30%	1.88
	4.15 V (≈ 35%–80%)	10%	1.56
		20%	1.61
		30%	1.61
BCR	4.0 V (≈ 15%–60%)	10%	3.34
		20%	–
		30%	–
	4.05 V (≈ 20%–70%)	10%	3.07
		20%	3.14
		30%	–
	4.1 V (≈ 30%–75%)	10%	3.63
		20%	3.76
		30%	3.97
	4.15 V (≈ 35%–80%)	10%	3.71
		20%	3.90
		30%	4.13

Table 5
Root mean square error (%) of the SOH estimation for different SOC errors over all the tested cells using time of constant current charging and mileage as inputs to the linear regression model.

SOC error (%)	Test cell			
	CC2	*BC*	*BCNP 1s*	*BCR*
−5	1.64	2.17	1.84	3.14
−2.5	1.06	1.75	1.75	3.41
−1	0.99	1.56	1.80	3.61
0	1.09	1.47	1.87	3.76
+1	1.29	1.41	1.96	3.91
+2.5	1.69	1.39	2.15	4.16
+5	2.48	1.55	2.55	4.60

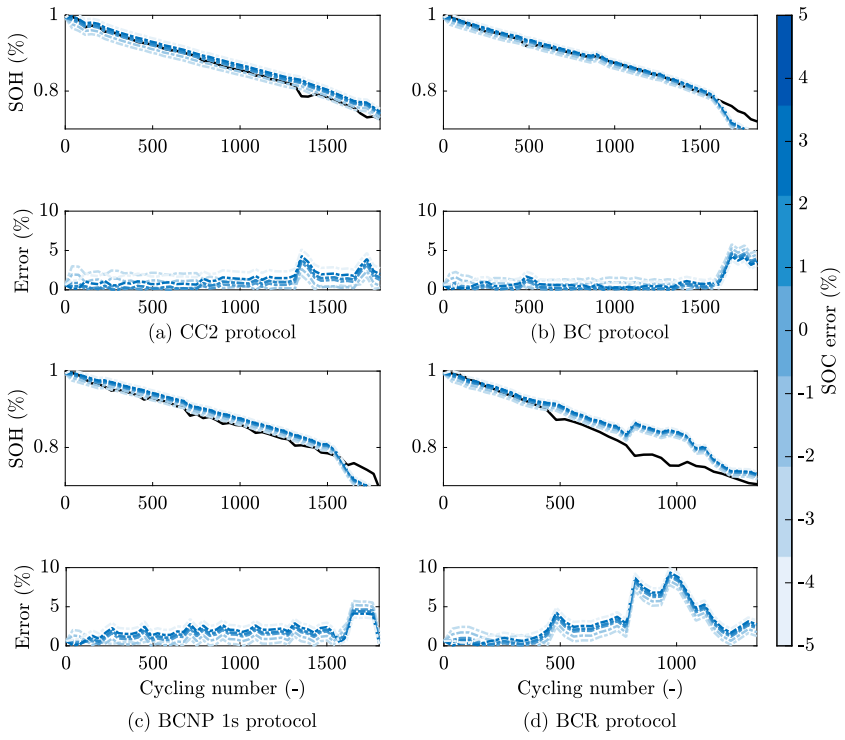

Fig. 8. SOH estimation results considering different SOC errors and using time of constant current charging and mileage as inputs to the linear regression model on the testing cells (a): constant current 2, (b): boost constant current, (c) pulse boost with 1s negative pulse, and (d): pulse boost with rest.

CRediT authorship contribution statement

Matteo Acquarone: Writing – original draft, Visualization, Software, Methodology, Investigation, Formal analysis, Data curation, Conceptualization. **Federico Miretti:** Writing – original draft, Supervision, Methodology, Investigation, Formal analysis, Data curation, Conceptualization. **Tiziano Alberto Giuliacci:** Software, Investigation, Formal analysis, Conceptualization. **Josimar Duque:** Writing – original draft, Resources, Data curation. **Daniela Anna Misul:** Supervision, Project administration. **Phillip Kollmeyer:** Writing – review & editing, Supervision, Project administration, Methodology, Investigation, Formal analysis.

Declaration of competing interest

The authors declare that they have no known competing financial interests or personal relationships that could have appeared to influence the work reported in this paper.

Appendix A. Supplementary data

Supplementary material related to this article can be found online at https://doi.org/10.1016/j.jpowsour.2024.235601.

Data availability

Data will be made available on request.

References

[1] O. Egbue, S. Long, Barriers to widespread adoption of electric vehicles: An analysis of consumer attitudes and perceptions, Energy Policy 48 (2012) 717–729, http://dx.doi.org/10.1016/j.enpol.2012.06.009, URL https://www.sciencedirect.com/science/article/pii/S0301421512005162.

[2] H. Wu, G. Alberts, J. Hooper, New market. New entrants. New challenges. Battery electric vehicles, Tech. rep., Deloitte, 2019, URL https://web.archive.org/web/20240119130240/https://www2.deloitte.com/content/dam/Deloitte/uk/Documents/manufacturing/deloitte-uk-battery-electric-vehicles.pdf.

[3] European Commission, Regulation of the European parliament and of the council on type-approval of motor vehicles and engines and of systems, components and separatetechnical units intended for such vehicles, with respect to their emissions and battery durability (euro 7) and repealing regulations (EC) no 715/2007 and (EC) no 595/2009, 2024, URL https://web.archive.org/web/20240119133027/https://eur-lex.europa.eu/legal-content/EN/TXT/PDF/?uri=CONSIL:ST_5142_2024_INIT.

[4] R. Xiong, Y. Pan, W. Shen, H. Li, F. Sun, Lithium-ion battery aging mechanisms and diagnosis method for automotive applications: Recent advances and perspectives, Renew. Sustain. Energy Rev. 131 (2020) 110048, http://dx.doi.org/10.1016/j.rser.2020.110048.

[5] M. Acquarone, P.G. Anselma, F. Miretti, D. Misul, Battery temperature aware equivalent consumption minimization strategy for mild hybrid electric vehicle powertrains, in: 2022 IEEE Vehicle Power and Propulsion Conference, VPPC, IEEE, 2022, pp. 1–6, http://dx.doi.org/10.1109/vppc55846.2022.10003225.

[6] M. Acquarone, F. Miretti, P.G. Anselma, D.A. Misul, Online temperature-aware equivalent consumption minimization strategy for mild hybrid electric powertrains, IEEE Trans. Veh. Technol. (2024) 1–13, http://dx.doi.org/10.1109/tvt.2024.3355181.

[7] H. Rahimi-Eichi, U. Ojha, F. Baronti, M.-Y. Chow, Battery management system: An overview of its application in the smart grid and electric vehicles, IEEE Ind. Electron. Mag. 7 (2) (2013) 4–16, http://dx.doi.org/10.1109/MIE.2013.2250351, URL https://ieeexplore.ieee.org/document/6532486.

[8] A. Pröbstl, S. Park, S. Narayanaswamy, S. Steinhorst, S. Chakraborty, SOH-aware active cell balancing strategy for high power battery packs, in: 2018 Design, Automation & Test in Europe Conference & Exhibition (DATE), 2018, pp. 431–436, http://dx.doi.org/10.23919/DATE.2018.8342048, URL https://ieeexplore.ieee.org/document/8342048, ISSN: 1558-1101.

[9] M. Kandidayeni, J.P. Trovão, M. Soleymani, L. Boulon, Towards health-aware energy management strategies in fuel cell hybrid electric vehicles: A review, Int. J. Hydrog. Energy 47 (17) (2022) 10021–10043, http://dx.doi.org/10.1016/j.ijhydene.2022.01.064, URL https://www.sciencedirect.com/science/article/pii/S0360319922001240.

[10] P.G. Anselma, P. Kollmeyer, J. Lempert, Z. Zhao, G. Belingardi, A. Emadi, Battery state-of-health sensitive energy management of hybrid electric vehicles: Lifetime prediction and ageing experimental validation, Appl. Energy 285 (2021) 116440, http://dx.doi.org/10.1016/j.apenergy.2021.116440, URL https://www.sciencedirect.com/science/article/pii/S0306261921000088.

[11] P.G. Anselma, Dynamic programming based rapid energy management of hybrid electric vehicles with constraints on smooth driving, battery state-of-charge and battery state-of-health, Energies 15 (5) (2022) 1665, http://dx.doi.org/10.3390/en15051665, URL https://www.mdpi.com/1996-1073/15/5/1665.

[12] X. Hu, L. Johannesson, N. Murgovski, B. Egardt, Longevity-conscious dimensioning and power management of the hybrid energy storage system in a fuel cell hybrid electric bus, Appl. Energy 137 (2015) 913–924, http://dx.doi.org/10.1016/j.apenergy.2014.05.013, URL https://www.sciencedirect.com/science/article/pii/S030626191400508X.

[13] S. Ebbesen, P. Elbert, L. Guzzella, Battery state-of-health perceptive energy management for hybrid electric vehicles, IEEE Trans. Veh. Technol. 61 (7) (2012) 2893–2900, http://dx.doi.org/10.1109/TVT.2012.2203836, URL https://ieeexplore.ieee.org/document/6214629.

[14] G.L. Plett, Dual and joint EKF for simultaneous SOC and SOH estimation, in: 21st Electric Vehicle Symposium (EVS21), 2005, p. 1.

[15] A. Allam, S. Onori, Online capacity estimation for lithium-ion battery cells via an electrochemical model-based adaptive interconnected observer, IEEE Trans. Control Syst. Technol. 29 (4) (2021) 1636–1651, http://dx.doi.org/10.1109/TCST.2020.3017566.

[16] N. Xu, Y. Xie, Q. Liu, Q. Liu, F. Yue, D. Zhao, A data-driven approach to state of health estimation and prediction for a lithium-ion battery pack of electric buses based on real-world data, Sensors (Basel) (2022).

[17] A. Severson Kristen, M. Attia Peter, J. Norman, P. Nicholas, J. Benben, Y. Zi, H. Chen Michael, A. Muratahan, K. Herring Patrick, F. Dimitrios, Z. Bazant Martin, J. Harris Stephen, C. Chueh William, D. Braatz Richard, Data-driven prediction of battery cycle life before capacity degradation, Nat. Energy (2019) http://dx.doi.org/10.1038/s41560-019-0356-8.

[18] J. Chen, M. Manivanan, J. Duque, P. Kollmeyer, S. Panchal, O. Gross, A. Emadi, A convolutional neural network for estimation of lithium-ion battery state-of-health during constant current operation, in: 2023 IEEE Transportation Electrification Conference & Expo (ITEC), 2023, pp. 1–6, http://dx.doi.org/10.1109/ITEC55900.2023.10186914, URL https://ieeexplore.ieee.org/abstract/document/10186914, ISSN: 2473-7631.

[19] M. Shi, J. Xu, C. Lin, X. Mei, A fast state-of-health estimation method using single linear feature for lithium-ion batteries, Energy 256 (2022) 124652, http://dx.doi.org/10.1016/j.energy.2022.124652.

[20] Z. Meng, K.A. Agyeman, X. Wang, Multi-segment state of health estimation of lithium-ion batteries considering short partial charging, IEEE Trans. Energy Convers. 38 (3) (2023) 1913–1923, http://dx.doi.org/10.1109/TEC.2023.3242876, URL https://ieeexplore.ieee.org/document/10038546.

[21] H. Meng, M. Geng, T. Han, Long short-term memory network with Bayesian optimization for health prognostics of lithium-ion batteries based on partial incremental capacity analysis, Reliab. Eng. Syst. Saf. 236 (2023) 109288, http://dx.doi.org/10.1016/j.ress.2023.109288, URL https://www.sciencedirect.com/science/article/pii/S095183202300203X.

[22] N. Wassiliadis, J. Schneider, A. Frank, L. Wildfeuer, X. Lin, A. Jossen, M. Lienkamp, Review of fast charging strategies for lithium-ion battery systems and their applicability for battery electric vehicles, J. Energy Storage 44 (2021) 103306, http://dx.doi.org/10.1016/j.est.2021.103306.

[23] R. Mathieu, O. Briat, P. Gyan, J.-M. Vinassa, Fast charging for electric vehicles applications: Numerical optimization of a multi-stage charging protocol for lithium-ion battery and impact on cycle life, J. Energy Storage 40 (2021) 102756, http://dx.doi.org/10.1016/j.est.2021.102756, URL https://www.sciencedirect.com/science/article/pii/S2352152X21004850.

[24] Y. Chu, R. Chen, T. Liang, S. Changchien, J. Chen, Positive/negative pulse battery charger with energy feedback and power factor correction, in: Twentieth Annual IEEE Applied Power Electronics Conference and Exposition, 2005. APEC 2005, in: APEC-05, Vol. 2, IEEE, 2005, pp. 986–990, http://dx.doi.org/10.1109/APEC.2005.1453109.

[25] B. Purushothaman, U. Landau, Rapid charging of lithium-ion batteries using pulsed currents: A theoretical analysis, J. Electrochem. Soc. 153 (3) (2006) A533, http://dx.doi.org/10.1149/1.2161580.

[26] U. Yayan, A.T. Arslan, H. Yucel, A novel method for SoH prediction of batteries based on stacked LSTM with quick charge data, Appl. Artif. Intell. 35 (6) (2021) 421–439, http://dx.doi.org/10.1080/08839514.2021.1901033.

[27] D. Zhang, Z. Wang, L. Peng, Z. Qin, Q. Wang, C. She, P. Bauer, Multi-step fast charging based state of health estimation of lithium-ion batteries, IEEE Trans. Transp. Electrif. (2023) 1, http://dx.doi.org/10.1109/tte.2023.3322582.

[28] F. Li, Y. Min, Y. Zhang, Y. Zhang, H. Zuo, F. Bai, State-of-health estimation method for fast-charging lithium-ion batteries based on stacking ensemble sparse Gaussian process regression, Reliab. Eng. Syst. Saf. 242 (2024) 109787, http://dx.doi.org/10.1016/j.ress.2023.109787.

[29] K.A. Severson, P.M. Attia, N. Jin, N. Perkins, B. Jiang, Z. Yang, M.H. Chen, M. Aykol, P.K. Herring, D. Fraggedakis, M.Z. Bazant, S.J. Harris, W.C. Chueh, R.D. Braatz, Data-driven prediction of battery cycle life before capacity degradation, Nat. Energy 4 (5) (2019) 383–391, http://dx.doi.org/10.1038/s41560-019-0356-8, URL https://www.nature.com/articles/s41560-019-0356-8.

[30] R. Zhou, R. Zhu, C.-G. Huang, W. Peng, State of health estimation for fast-charging lithium-ion battery based on incremental capacity analysis, J. Energy Storage 51 (2022) 104560, http://dx.doi.org/10.1016/j.est.2022.104560.

[31] Y. Fan, H. Wang, Y. Zheng, J. Zhao, H. Wu, K. Wang, S. Yang, X. Tan, A novel state-of-health estimation method for fast charging lithium-ion batteries based on an adversarial encoder network, J. Energy Storage 63 (2023) 107087, http://dx.doi.org/10.1016/j.est.2023.107087.

[32] J. Duque, P.J. Kollmeyer, M. Naguib, Battery aging dataset for 15 minute fast charging of samsung 30t cells, 2023, http://dx.doi.org/10.5683/SP3/UYPYDJ.

[33] J. Duque, P.J. Kollmeyer, M. Naguib, A. Emadi, Battery dual extended Kalman filter state of charge and health estimation strategy for traction applications, in: 2022 IEEE Transportation Electrification Conference & Expo, ITEC, IEEE, 2022, pp. 975–980, http://dx.doi.org/10.1109/itec53557.2022.9813961.

[34] S.B. Vilsen, D.-I. Stroe, Battery state-of-health modelling by multiple linear regression, J. Clean. Prod. 290 (2021) 125700, http://dx.doi.org/10.1016/j.jclepro.2020.125700.

[35] J. Duque, P.J. Kollmeyer, M. Naguib, Battery aging dataset for 15 minute fast charging of samsung 30T cells, 2023, http://dx.doi.org/10.5683/SP3/UYPYDJ.

[36] H. Feng, Y. Liu, An approach for fast-charging lithium-ion batteries state of health prediction based on model-data fusion, J. Electrochem. Energy Convers. Storage 21 (2) (2024) http://dx.doi.org/10.1115/1.4062990.

[37] D. Yang, X. Zhang, R. Pan, Y. Wang, Z. Chen, A novel Gaussian process regression model for state-of-health estimation of lithium-ion battery using charging curve, J. Power Sources 384 (2018) 387–395, http://dx.doi.org/10.1016/j.jpowsour.2018.03.015.

[38] S. Jo, W. Kim, J. Kim, K.-S. Kim, Study on actual ah-throughput-based health indicator of battery module consisting of inconsistent cells for its second life, Electron. Lett. 58 (15) (2022) 588–590, http://dx.doi.org/10.1049/ell2.12523.

[39] Z. He, X. Shen, Y. Sun, S. Zhao, B. Fan, C. Pan, State-of-health estimation based on real data of electric vehicles concerning user behavior, J. Energy Storage 41 (2021) 102867, http://dx.doi.org/10.1016/j.est.2021.102867.

[40] H. Peng, F. Long, C. Ding, Feature selection based on mutual information criteria of max-dependency, max-relevance, and min-redundancy, IEEE Trans. Pattern Anal. Mach. Intell. 27 (8) (2005) 1226–1238, http://dx.doi.org/10.1109/tpami.2005.159.

[41] MATLAB, Fit linear regression model, 2023, URL https://it.mathworks.com/help/stats/fitlm.html.

[42] K. Movassagh, A. Raihan, B. Balasingam, K. Pattipati, A critical look at Coulomb counting approach for state of charge estimation in batteries, Energies 14 (14) (2021) 4074, http://dx.doi.org/10.3390/en14144074.